Inverse scattering problem for optical coherence tomography

Oscar P. Bruno and Julian Chaubell

Applied and Computational Mathematics, 217-50 California Institute of Technology, Pasadena, California 91125

Received May 29, 2003

We deal with the imaging problem of determining the internal structure of a body from backscattered laser light and low-coherence interferometry. Specifically, using the interference fringes that result when the backscattering of low-coherence light is made to interfere with the reference beam, we obtain maps detailing the values of the refractive index within the sample. Our approach accounts fully for the statistical nature of the coherence phenomenon; the numerical experiments that we present, which show image reconstructions of high quality, were obtained under noise floors exceeding those present for various experimental setups reported in the literature. © 2003 Optical Society of America

OCIS codes: 030.0030, 110.1650, 110.0180, 180.3170.

Optical coherence tomography (OCT) is a noninvasive imaging technique based on the use of light sources exhibiting a low degree of coherence. Low-coherence interferometric microscopes have been successful in producing internal images of thin pieces of biological tissue. Typically samples of the order of 1 mm in depth have been imaged, with a resolution of the order of 10 to 20 μm in some portions of the samples.[1,2] These OCT images resulted from renderings of the intensities of interference fringes as functions of the position of the light focus within the sample; quite generally, limited postprocessing of these data has been used. In this Letter we present a computational technique that, by use of OCT interferometric data from a given layered medium, can produce significantly more quantitative and detailed output than previous methods, namely, the complete refractive-index maps of the corresponding sample, even for media containing a large number of layers. Once it is obtained, a straightforward display of the refractive-index map yields, in particular, an image of the internal structure of the sample. The present techniques should be extendable to cases in which layers are not planar through the use of multiple points of light collection.

Methods have been reported that produce refractive-index maps from OCT data for samples containing a few parallel layers.[1,3–5] In these methods refractive indices and layer widths are obtained sequentially by means of two different types of measurement: (1) The sample position is varied with the reference arm shut until an intensity peak is obtained, and (2) the shutter is opened and the mirror is moved to a position of maximum contrast for the interference fringes. This procedure thus requires data processing at collection time. The technique that we introduce in this Letter, in turn, can produce quantitative refractive-index maps within samples containing thousands of layers (with parallel planar interfaces) from backscattering interference fringes only, without processing at data collection time. As in the techniques reported in Refs. 1 and 3–5, the OCT technique under consideration is based on the use of a low-coherence light source and a Michelson interferometer, as shown in Fig. 1. As the sample to be imaged is placed in one arm of the interferometer, the light reflected from the reference mirror and the light backscattered from the sample are combined at the detector; the intensity of the interference fringes that result as the position of the reference mirror is varied is the information from which the interior image of the sample is to be obtained. The total optical intensity received by the detector is given by[6] $I_D = \int_S \langle |u_r(P,t) + u_s(P,t)|^2 \rangle_T \, dS_p = 2\Sigma + \int_S \langle |u_r(P,t)|^2 \rangle_T + \langle |u_s(P,t)|^2 \rangle_T \, dS_p$; $*$ denotes complex conjugation; $\langle \ldots \rangle_T$ denotes time averages; P is a point on the detector; dS_P is the element of the area on the lens receiving the combined field; $u_r(P,t)$ and $u_s(P,t)$ represent the fields backscattered from the reference arm and the sample arm, respectively; and $\Sigma = \mathrm{Re}[\int_S \langle u_r(P,t) u_s^*(P,t) \rangle_T dS_P]$ denotes the correlation between the reference and the scattered field averaged over the surface, S, of the detector. The correlation Σ can be re-expressed in terms of the power spectral density, $S(\omega)$, of the light source[6] and the refractive properties of the sample. Indeed, let us denote as $\hat{u}^{\mathrm{src}}(\omega) = E_0(\omega)\exp(ikz)$ the electric field (a beam parallel to a z axis, $k = \omega/c$) generated by the superluminescent diode source at frequency ω. As it travels through the splitter and the lens toward the sample, each ray in this beam acquires an angle of incidence θ; see Fig. 1. Each such ray is multiply reflected and refracted by the various interfaces within the sample (according to Snell's law for amplitudes

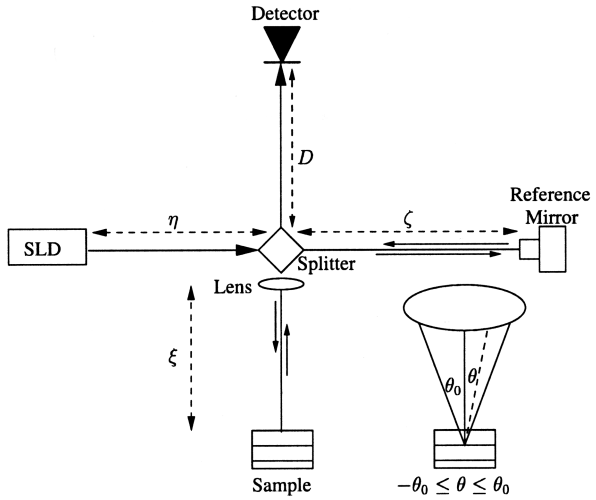

Fig. 1. Optical coherence microscope. SLD, superluminescent diode.

0146-9592/03/212049-03$15.00/0

and angles), and thus the incident beam gives rise to infinitely many rays scattered away from the sample.

Each one of these infinitely many rays produces a certain degree of interference as it combines with the reference beam at the detector. After passing through the lens and the splitter, a given ray arrives at a point P on the detector and contributes an electric field $\hat{u}_s(P, \omega)$. The electric field contributed at point P by the reflection from the mirror, on the other hand, equals $\hat{u}_r(P, \omega) = \frac{1}{4}\exp[ik(D + 2\zeta + \eta)]$, which, of course, is constant with respect to P, where D, ζ, η, and ξ are illustrated in Fig. 1. With these notations the correlation Σ becomes

$$\sqrt{2\pi}\,\Sigma = \mathrm{Re}\left\{\int_S \int_{-\infty}^{\infty} S(\omega)\hat{u}_r{}^*(P, \omega)\hat{u}_s(P, \omega)\mathrm{d}\omega\mathrm{d}S_p\right\}. \tag{1}$$

As is common practice, our work assumes a Gaussian power spectral density $S(\omega)$ and its corresponding complex degree of coherence function $\gamma(\tau)$; see, e.g., Ref. 6. Experimentally, Σ can be obtained by (1) measurements resulting from blocking, in turn, the sample and reference arms to obtain, respectively, the intensities of the reference and sample fields, followed by (2) subtraction of the sum of these quantities from I_D. Note that this two-step procedure does not require data processing at collection time.

Our numerical method determines the distributions of refractive indices within the sample from sequences of values of the correlation Σ (as a function of ξ for fixed ζ). To illustrate our discussion we first consider Fig. 2, which displays the absolute value of Σ as a function of $\zeta - \xi$ for a sample consisting of ten 100-μm layers—although with the wavelengths considered here, layers as fine as 20 μm could be resolved—and with refractive indices n of 1.3–1.4; clearly, one can obtain measurements of this function by moving the sample to appropriate sequences of points in space. The marked peaks in Fig. 2 correspond to light scattered by the interfaces.

For example, the second peak in the top part of Fig. 2 arises from the interference of light scattered by the second interface; the line joining the circles in the bottom portion of Fig. 2 shows an enlarged view of this second peak. One can see that these peaks have a definite structure. Figure 2 (bottom) also shows a fine sampling of the interference fringes created by the second interface. Our method utilizes the coarsely sampled values contained in such peak structures [shown by the circles in Fig. 2 (bottom)] to determine the refractive-index distributions within the sample. To describe our method let us call $d_1, \ldots, d_j$ and $n_1, \ldots, n_j$ the widths of layers $k = 1, \ldots, j$, and let us assume that n_1 has already been obtained (the method used to determine n_1 is described below). Then, calling d and n the unknown values of d_1 and n_2, respectively, and using the known value n_1 of the refractive index of the first layer, we construct the nonlinear function $F = F(n, d)$ given by the sum of the squares of the differences between measured data points on the second correlation peak and the corresponding values calculated under the assumption that the thickness and refractive index of the first and second layer, respectively, are d and n. The important point here is that, because of the coherence properties of the light used, both the actual and the calculated correlations, and therefore the function F, do not depend, except for negligible contributions, on either the refractive indices $n_3, \ldots, n_j$ or the widths $d_2, \ldots d_j$: The light reflected by the subsequent interfaces has a much longer optical path than that of the reference beam. Clearly, the minimization of function F with respect to d and n produces the desired values of d_1 and n_2. As described below, this minimization problem can be treated effectively by means of the Gauss–Newton method.[7] [We note here that the data used for evaluation of the width and the refractive index do not contain the complete details of the interference fringes. Full interference fringes corresponding to the second peak are displayed in Fig. 2 (bottom)]. Clearly, this procedure can be continued, once d_1 and n_2 are known, by construction and minimization of a second nonlinear function, this time associated with the third peak in Fig. 2, to determine d_2 and n_3 and so on, until the complete set of refractive indices and widths has been determined. It remains for us to describe our method for determination of the refractive index n_1. As can be easily understood, the index n_1 can be obtained from the first peak by means of a simplified version of the algorithm described above: The details of the first peak depend on only the refractive index of the first layer.

The minimization procedure requires calculation of the quantity F, and thus Σ, for assumed refractive indices and layer widths as a function of $\zeta - \xi$. An exact calculation of this function would be prohibitively expensive in terms of computing time. Fortunately,

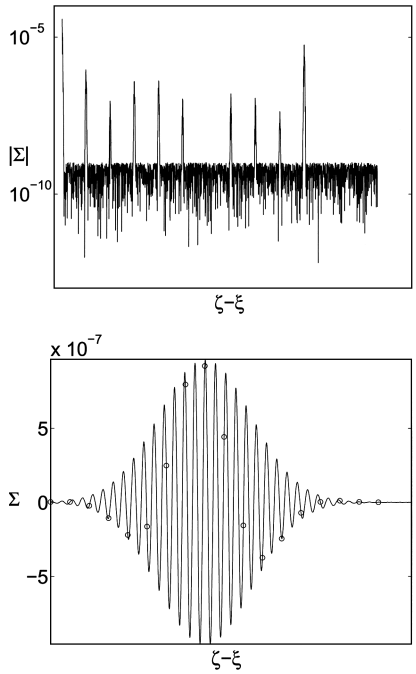

Fig. 2. Interference fringes. Top, absolute value of the correlation function Σ; bottom, finely sampled second spike, with circles corresponding to the coarse samples displayed at the bottom.

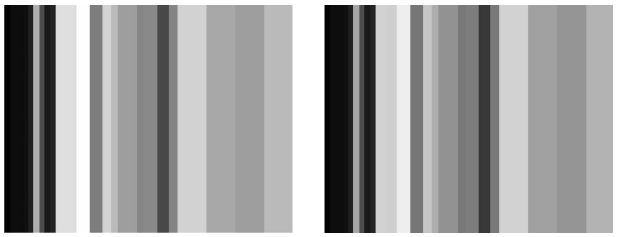

Fig. 3. Layered structure. Left, original image; right, reconstruction.

the low-coherence properties of superluminescent diode light allow for evaluation of Σ in an extremely simple and fast manner. To simplify the evaluation of the integral in Eq. (1) we use the fact that, at each point P, the product $\hat{u}_r{}^*(P, \omega)\hat{u}_s(P, \omega)$ is given by a linear combination of (a large number of) exponentials, one for each of the backscattered rays arriving at P whose total optical path is sufficiently close to that of the reference beam. This restriction reduces enormously the number of exponential functions that need to be considered in this calculation. For each of these exponentials the corresponding integral can be obtained directly from the complex degree of coherence of the source $\gamma(\tau) = 1/2\pi \int_{-\infty}^{\infty} S(\omega)\exp(-i\omega\tau)\mathrm{d}\omega$. Integration of this quantity over the area S_P of the detector, finally, produces the average correlation, Σ. The benefits of this approach are significant: On a 700-MHz PC, the direct evaluation of Σ at 2200 scanning points takes 16 min, whereas the corresponding evaluation through the use of the complex degree of coherence requires only a 25-s run.

A difficulty arises in the solution of the problem of minimization of the nonlinear function F mentioned above, since the Gauss–Newton method generally converges to a local minimum only, and local minima are ubiquitous in our problem. An important task is, then, to find appropriate starting points from which the Gauss–Newton method converges to the global minimum. Our strategy for selection of starting points is a central element of our approach. This selection strategy is based on the structure of the function F to be minimized, which exhibits the following characteristics in every case: parabolic behavior as a function of the real part n of the refractive index and oscillatory behavior as a function of thickness variable d. As one can check, the oscillations exhibited by F as a function of d have an approximate period of $p = \lambda/2n^{\mathrm{prev}}$, which n^{prev} denotes the refractive index of the previous layer and λ is the wavelength of the incident beam. This structure allows us to use simple one-dimensional minimization problems to obtain excellent starting guesses. Indeed, a one-dimensional Newton minimization in the n direction starting from an arbitrary point will necessarily result in a point within the basin of attraction of a local minimum of $F(n, d)$. Two-dimensional minimization in (n, d) starting from this point will thus lead to a local minimum. Once such a local minimum point is found, moving along the d direction with steps of size p will provide new sequences of initial guesses, one in the basin of attraction of each one of the relevant local minima. Use of the two-dimensional Newton method around these points then results in a sequence of local minima, and thus, by comparison, the global minimizer—the desired values of the refractive index and width of the current layer—can be obtained.

To demonstrate the performance of our algorithms we consider the layered structure depicted in the left-hand portion of Fig. 3, which consists of 25 layers of various widths within the 1-mm sample. A synthetic experimental backscattered field obtained by direct computation was used, and an error was added to simulate the experimental noise floor; the added error was taken to be random and of the order of 10^{-4} times the largest interference intensity arising in the computation; see Fig. 2 (top). This noise level is much larger than in the various noise bars reported in the literature.[8] The center wavelength and bandwidth of the laser were taken to be $\lambda = 850$ nm and $\Delta\lambda = 70$ nm, respectively. The N.A. of the focusing lens was taken to be 0.108. The absorption κ of the actual sample was taken to vary randomly from 0 to 10^{-4}, with an average of 0.6×10^{-4}; we solve the inverse problem by assuming that the refractivities that were sought have an imaginary part (absorption) equal to the average value 0.6×10^{-4}. The grayscale maps in Fig. 3 represent the real part n of the refractive index. The darkest portion corresponds to $n = 1.33$, and the lightest corresponds to $n = 1.64$. In Fig. 3 (right) we present the reconstruction resulting from our algorithm, a clear image of the interior of the sample. This reconstruction was produced by a 36-min calculation on a 700-MHz PC.

Support provided by TRW, the U.S. Air Force Office of Scientific Research, and the National Science Foundation is gratefully acknowledged. O. P. Bruno's e-mail address is bruno@acm.caltech.edu.

References

1. G. J. Tearney, M. E. Brezinski, J. F. Southern, B. E. Bouma, M. R. Hee, and J. G. Fujimoto, Opt. Lett. **20,** 2258 (1995).
2. J. W. Hettinger, M. de la Peña Mattozzi, W. R. Meyers, M. E. Williams, A. Reeves, R. L. Parsons, R. C. Haskell, D. C. Petersen, R. Wang, and J. I. Medford, Plant Physiol. **123,** 3 (2000).
3. T. Fukano and I. Yamaguchi, Opt. Lett. **21,** 1942 (1996).
4. M. Haruna, M. Ohmi, T. Mitsuyama, H. Tajiri, H. Maruyama, and M. Hashimoto, Opt. Lett. **23,** 966 (1998).
5. Y. Watanabe and I. Yamaguchi, Appl. Opt. **41,** 2414 (2002).
6. J. W. Goodman, *Statistical Optics* (Wiley, New York, 1985).
7. G. Byrne and Ch. Hall, *Numerical Solution of Systems of Nonlinear Algebraic Equations* (Academic, New York, 1973).
8. M. Yadlowsky, J. Schmitt, and R. Bonner, Appl. Opt. **34,** 5699 (1995).